RAPID COMMUNICATIONS IN MASS SPECTROMETRY
Rapid Commun. Mass Spectrom. **12**, 1236–1240 (1998)

Angle and Energy Distributions of Neutral Atoms Sputtered from $Ni_3Al(100)$

Bruce V. King[1], C. Zimmermann[1], Donald E. Riederer[2]†, Scott W. Rosencrance‡, Barbara J. Garrison[2] and Nicholas Winograd[2]*

[1]Department of Physics, University of Newcastle, Callaghan 2308, Australia
[2]Department of Chemistry, The Pennsylvania State University, University Park, PA 16802, USA

The energy and angular distributions of Ni and Al atoms sputtered from $Ni_3Al(100)$ by 8 keV Ar^+ have been measured using multiphoton resonance ionization detection. The Al atoms, which originate entirely from the top atomic layer of $Ni_3Al(100)$, are predominantly sputtered along close packed <110> directions. On the other hand the sputtered Ni flux, which arises from both the first and second layers, has a large component normal to the surface. Molecular dynamics computer simulations agree well with experimental results and suggest that the normal emission of Ni atoms arises primarily from second-layer atoms. © **1998 John Wiley & Sons, Ltd.**

Received 24 April 1998; Revised 22 July 1998; Accepted 24 July 1998

Energy transfer processes that lead to the desorption of atoms and molecules from ion bombarded surfaces involve a complex sequence of nuclear collisions. There have been many spirited debates through the years related to questions about the detailed nature of these collisions. Various strategies ranging from energy transport theories[1] to Monte Carlo simulations[2] have been exploited to gain a certain level of understanding. Of special interest is the case of single crystal metal targets where atoms are observed to eject along specific crystallographic directions. For these systems, molecular dynamics (MD) computer simulations have been successful at reproducing experimental measurements of the energy and angle distributions of neutral atoms.[3] This agreement is encouraging since comparisons at this level of detail confirm a high degree of reliability for the MD model.

One aspect of the desorption process has involved the depth of origin of the ejected atom.[1–4] Computer simulations have shown that for copper single crystals >90% of the particles are emitted from the top layer.[5] More recent models suggest that for fcc single crystals, some 2nd layer ejection can occur through a ring of top-layer atoms and is observed primarily at an angle normal to the surface plane.[6–8] Experimental tests of this prediction have been difficult since there is no way to distinguish between layers in a monoelemental target. One particularly elegant experiment involved the measurement of the yield of Ru from Ru{0001} as it is systematically covered with a monolayer of Cu.[9] The results show that the particles do arise almost exclusively from the top layer, although no information regarding the take-off angle of the few atoms emitted from the second layer were reported. Moreover, the overlayer of Cu had an undefined relationship to the Ru substrate.

Single crystal metallic alloys represent an interesting model system for these types of studies. It is technically feasible to prepare compounds that have well-defined numbers of atoms of a specific type in a specific layer. Moreover, the atomic configurations can be precisely determined using a variety of spectroscopic approaches.[10–12] These attributes are critical to designing experiments that can be compared with theory since important input parameters for molecular dynamics computer simulations are the mass and crystallographic location of each atom. The calculations are also possible since more reliable interaction potential surfaces have become available which are derived from many-body approaches such as the embedded atom method. To our knowledge, no sputtering experiments have been reported on single-crystal alloy surfaces.

In this paper, we examine the energy and angle distributions of Ni and Al atoms emitted from a $Ni_3Al(001)$ single crystal target. This material exhibits a bulk termination in which the top layer is 50% Ni and 50% Al while the second layer is 100% Ni. The results show that emission of Ni atoms in off-normal directions is reduced by more than two-fold relative to the normal direction when compared to pure Ni(100). Parallel molecular dynamics computer simulations using approximate interaction potentials for Ni_3Al yield virtually identical information. These changes in angular distribution are expected if the particles emitted in the normal direction originate primarily from the second layer. The experiments and calculations also show that the angular distributions of Al atoms are consistent with the known crystal structure of $Ni_3Al(100)$ and further confirm that desorption in off-normal directions arises from first layer atoms channeled through open crystallographic directions of the lattice.

EXPERIMENTAL

Laser postionization was used to measure the angular distributions of Ni and Al atoms sputtered from $Ni_3Al(100)$. This technique has two advantages. First, it probes the atom flux directly and avoids the matrix problems inherent in

*Correspondence to: N. Winograd, Department of Chemistry, The Pennsylvania State University, University Park, PA 16802, USA.
†Present address: Department of Chemistry, 123 Chemistry Building, University of Missouri, Columbia, MO 65211, USA.
‡Present address: 731 Beaver Drive, Naperville, IL 60540, USA.
Contract/grant sponsor: National Science Foundation.
Contract/grant sponsor: IBM Corporation, SUR program.

CCC 0951–4198/98/181236–05 $17.50

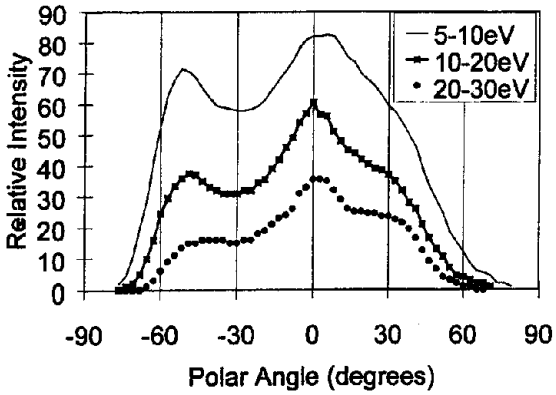

Figure 2. Experimental measurement of the angular distribution of Ni atoms sputtered from the $Ni_3Al(100)$ surface by normally incident 8 keV Ar^+ as a function of ejection energy. Negative angles represent the angle from the normal along the <100> azimuth whereas positive angles represent the angle from the normal along the <110> azimuth. All measured angles were recorded within a $\pm$ 7.5° interval around the appropriate azimuth.

RESULTS AND DISCUSSION

Experimental and calculated energy-resolved angular distributions for Ni and Al atoms emitted from ion-bombarded $Ni_3Al(100)$ are examined along specific azimuthal directions as shown in Fig. 1. The first direction is the <110> direction involving close-packed rows of alternating Al and Ni atoms, and the other direction is the <100> direction involving alternating rows of Al and Ni atoms. In general, a higher intensity of particles is observed along the <100> direction since the atoms are spaced further apart ($2a_o/\sqrt{2}$) and it is easier for desorbing atoms to escape the surface without blockage.

Experimental measurements

The polar angle distributions of Ni and Al sputtered along the <100> and <110> azimuths are shown in Figs 2 and 3. The Ni angular distributions exhibit the same three broad peaks as seen for Ni(100) although their relative intensities are markedly different. Specifically, the peak at a polar angle $\theta = 0°$ is more than twice as intense as that reported for Ni(100).

The peak along the <100> azimuth shifts slightly toward the normal as the kinetic energy of the desorbed Ni atoms increases, whereas the peak position along the <110> azimuth is less sensitive to kinetic energy. This effect was also noticed for Ni(100) and arises from the increased dominance of purely first layer scattering along <100> for higher energy processes. These mechanisms tend to yield desorption at angles closer to the normal than those that involve collisions with subsurface atoms.

The corresponding energy-resolved angular distribution of desorbed Al atoms is shown in Fig. 3. The major characteristic of this distribution is that it lacks any resolvable feature at $\theta = 0°$. As we shown in the next section, this effect is due to the fact that normal emission arises primarily from second-layer atoms and $Ni_3Al(100)$ has no second-layer Al atoms.

Overall, Figs 2 and 3 show similarities with previous results for Ni(100)[6] if the fractions of Ni and Al atoms from the first and second layers are taken from the known $Ni_3Al(100)$ surface structure. Quantitative agreement is harder to obtain. Figure 4 in Ref. 6 shows that the peak in the <100> azimuth in the Ni(100) simulated spectrum comes entirely from the first layer, the normal peak 39% from the first layer and 61% from the second layer and the peak in the <110> azimuth 78% from the first layer and 22% from the second layer. When these fractions are scaled for the atomic concentrations in $Ni_3Al(100)$ (first layer 50% Ni, 50% Al and second layer 100% Ni) then the expected peak heights in the 3 directions (<100>, normal, <110>) for $Ni_3Al(100)$ should be in the ratio 2.9:0.55:1 for Al and 1.9:1.4:1 for Ni. Experimentally (Figs 2 and 3) it can be seen that the normal ejection component for Ni is higher than the above ratios would suggest. This same trend was found previously for Ni(100) (Fig. 3 in Ref. 6) where the experimental peak for normal ejection was 50% higher, relatively, than the peak in the simulation. The second point of difference is that the peak along the <100> azimuth for Al ejection is only slightly greater than the <110> peak, not in the ratio 2.9:1 calculated above. Hence, although this simplified explanation leads us in the correct direction, a more sophisticated approach involving molecular dynamics calculations is needed to yield a more quantitative picture. These calculations are described in the next section.

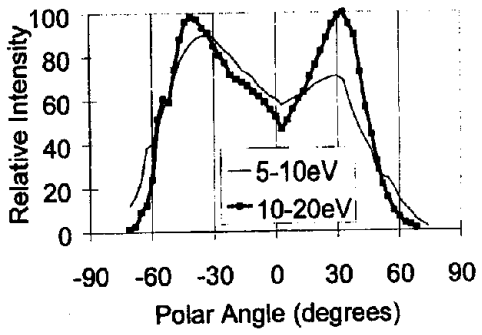

Figure 3. Experimental measurement of the angular distribution of Al atoms sputtered from the $Ni_3Al(100)$ surface as a function of ejection energy. Directions are the same as in Fig. 2.

Calculations

Molecular dynamics calculations have been shown to accurately reproduce the measured energy and angular distributions of atoms ejected due to energetic particle bombardment. In particular, there is excellent agreement between calculated and measured distributions for clean Ni(100).[6] In order to examine the sputtering of the alloy system we would prefer to use potentials that have been previously calibrated by us for use in these energetic processes. Unfortunately, the MD/MC-CEM[17,18] potentials cannot be used for alloys (A.E. DePristo, private communication) and the Sandia EAM potentials[19] have not been developed for the Ni–Al alloy system. The many-body potentials that exist for Ni–Al alloys[20,21] have not yet been calibrated by us for use in sputtering MD calculations. Since we are mainly interested in examining the difference between the energy and angular distributions of pure Ni and the Ni_3Al alloy and to see if the predicted dependence on depth of origin can be seen in the MD simulations, we have chosen to use the EAM many-body potential for Cu_3Au, since this structure is similar to Ni_3Al. This strategy allows a qualitative test of our hypothesis and will provide a guide as to the influence of mass in the predicted distributions.

techniques such as secondary ion mass spectrometry. Second, it is very sensitive so that measurements can be made on an effectively undamaged surface. The experimental apparatus, which has been described in more detail previously[13,14] comprises a UHV chamber (base pressure 2.5×10^{-10} mbar) equipped with low energy electron diffraction (LEED) as well as an 8 keV Ar^+ ion source which could be operated in either pulsed or continuous mode. A 300 ns pulse of normally incident 8 keV Ar^+ ions, focused to a mm spot on the target, was used to sputter Al or Ni atoms into the path of a ribbon beam from a tunable dye laser.

The dye laser using Rhodamine R640 dye was pumped at 30 Hz by a Nd:YAG laser. Three 2-photon, one-color ionization schemes were used to probe the sputtered atoms. The 308.3 nm light was used to excite Al ($^2P_{1/2} - {}^1D_{3/2}$), while 303.9 nm and 302.3 nm light were used to excite the Ni D (a^3D_3–Y^3F_3) fine structure state, respectively. It has previously[13] been shown that, for sputtered Ni atoms, that the signal from the a^3D_3–Y^3F_3 transition is higher than that from the a^3F_4–Y^3F_3 transition even though the F state is the ground state. The laser beam was focused by a cylindrical lens to give a beam of rectangular cross-section, approximately 1 cm × 0.1 cm, directly above the target. At the typical power levels measured for the laser light, 30 mW, the power density in the laser beam is insufficient to saturate the transition. Atoms which are ejected at oblique angles to the surface, however, spend more time in the laser beam and so have a higher probability of being ionized compensating for the decreased ionization cross-section away from the laser focus.

The photoions are extracted into an 8 cm long true-of-flight (TOF) instrument and accelerated onto a 75 mm diameter microchannelplate and phospor screen. The two dimensional distribution of ions striking the detector is imaged using a camera and framegrabber into a personal computer. By collecting a series of images with varying time delays between the ion and laser pulses, the energy and angular distributions could be decoupled.[14] Secondary ions from the sputtered surface were rejected by pulsing the grids of the TOF with high voltages. The sputtering ion beam, however, did generate secondary ions as it passed through one of the grids in the TOF. The background from these ions prevented Al photoions with more than 10 eV or Ni photoions with more than 30 eV from being measured.

The $Ni_3Al(100)$ crystal used in this work has previously been used for low energy ion scattering studies on $Ni_3Al(100)$.[15,16] The crystal was cleaned by repeated cycles of sputtering with 10 mA/cm^{-2} 8 keV Ar^+ ions followed by annealing at 1000 K. Finally the surface was flash annealed to 1200 K. This procedure has previously been found to give a clean ordered surface.[15,16] Indeed, the LEED exhibited a very sharp c(2 × 2) ordered surface.

It is important that the energy and angle-resolved measurements be made on a clean undamaged surface. This is ensured in two ways. First, all experiments were performed within 40 minutes of cleaning because, although LEED measurements did not show any degradation, there was a small change in the angular distributions at longer times. Oxygen adsorption is known to form a disordered 1 ML thick AlO_x layer[16] (where $1 < x < 2$) at least at high substrate temperatures. Second, since the $Ni_3Al(100)$ surface is known to preferentially lose Al under ion bombardment, a complete angular scan was taken using an ion dose of less than 10^{11} ions/cm^2.

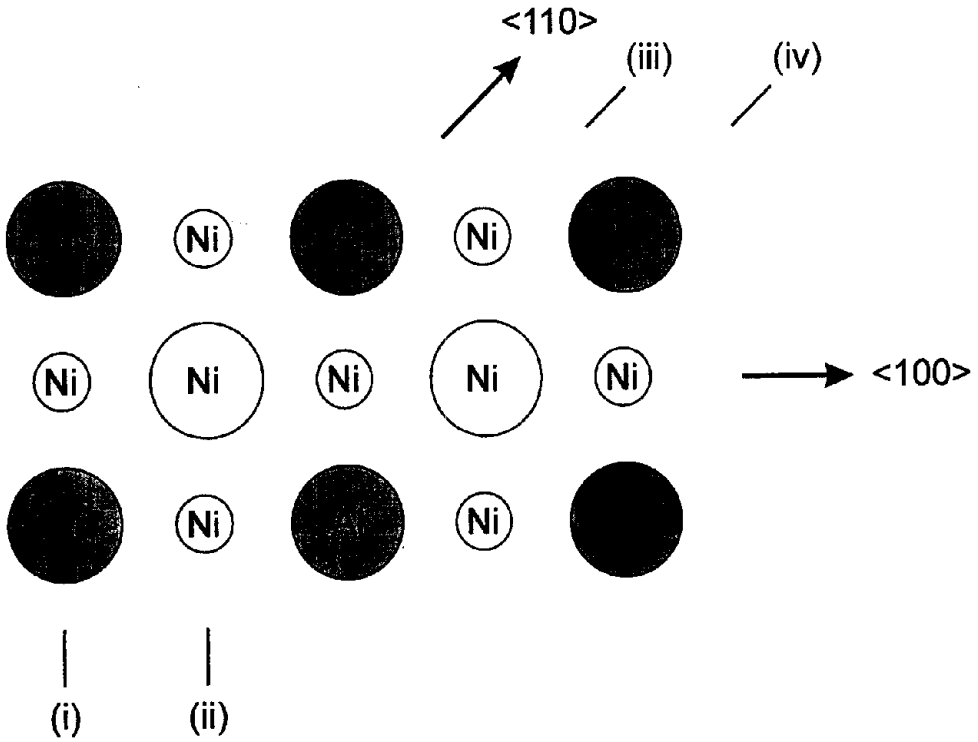

Figure 1. Plan view of the $Ni_3Al(100)$ surface. Al atoms are denoted by dark circles while Ni atoms are denoted by open circles. The plan view shows that the top layer is 50% Al and 50% Ni (large circles) whereas the second layer is 100% Ni (small circles). Cuts along the <100> azimuth can contain either (i) 50% Ni, 50% Al atoms or (ii) 100% Ni atoms. In the <110> azimuth, cut (iii) which contains 100% Ni atoms terminates $a_o/2$ below the surface layer whereas the cut (iv), containing 50% Ni 50% Al, terminates on the surface.

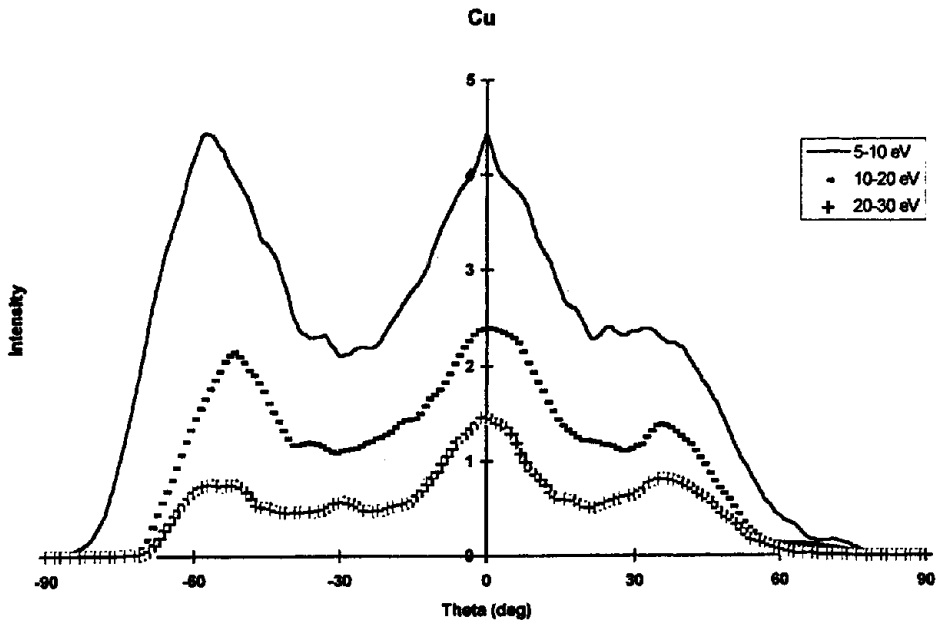

Figure 4. Calculated energy and angle distributions for Cu atoms sputtered from Cu_3Au with the Al mass substituted for the Au mass. Directions are the same as in Fig. 2.

The MD calculations performed here are identical to those previously reported for the clean Ni system.[6] The crystallite size consists of 9 layers of 200 atoms each. The odd numbered layers have 50% Cu and 50% Au and the even numbered layers have 100% Cu. The Cu_3Au EAM potential is used to approximate the substrate interactions. We make one adjustment, however, in that we substitute the mass of Al for that of Au. As described previously[22] a repulsive Moliére interaction was splined to the EAM potential in order to give it a sufficiently repulsive inner wall at close internuclear separation. The incident Ar has 3 keV of kinetic energy and Moliére potentials are used for the Ar–substrate interactions where the atomic numbers of Cu and Au are used. A total of 3000 Ar impacts were run on this alloy system in order to generate sufficient statistics to plot meaningful energy and angular distributions.

As calibration and for comparison purposes we also completed 1000 different Ar impacts on a clean Cu system with the EAM potential in order to ascertain that the distributions look like the published ones for pure Ni(100) in which the MD/MC-CEM potential was used.[6] These Cu EAM distributions do have the same general characteristics as the Ni MD/MC-CEM distributions, reinforcing the notion that the crystal structure is an important factor in controlling the development of the collision cascade. We also plotted artificial alloy distributions (not shown) by using 50% intensity from the first layer to represent Al and 50% intensity from the first layer and 100% intensity from the second layer to represent Ni. These distributions are not meant to represent the experimental data shown in Figs 2 and 3, but are used to assess the probability of second layer desorption in the normal direction. In addition, we performed simulations for Cu_3Au. These distributions exhibit very similar trends as discussed below for the system with artificial mass replacement.

Energy resolved angular distributions from these calculations are shown in Figs 4 and 5 for the Cu and Au (with Al mass) components, respectively. (For convenience we use the labels of Cu and Al even though that is not quite technically correct.) Consider first the Cu distributions shown in Fig. 4. For particles with 5–10 eV, the peak at $\theta = 0°$ is as intense as the peak along the <100> direction. This is not similar to clean Ni(100) even in the artificial distributions in which we use only 50% of the first layer intensity and 100% of the second layer intensity. Since the simulations yield absolute numbers, we clearly see that the peak at $\theta = 0°$ has increased by ~50% and the peak along the <100> direction has decreased by a factor of ~2 from the artificial distributions. The peak along the <110> direction is small in both cases and becomes less obvious with a large peak at $\theta = 0°$.

It has been proposed above that the peak at $\theta = 0°$ is composed primarily of second layer atoms. These MD simulations clearly support this claim. In fact, the amount of second layer ejection is actually larger for the alloy than for the pure material. Thus, the increase in the peak at $\theta = 0°$ in the alloy as compared to the pure Ni is due not only to a decreased statistical importance of the first layer ejection but also to an increase of second layer ejection. One hypothesis for the increased second layer ejection is that the mass mismatch between the two components slightly inhibits energy from escaping the near surface region and going into deeper parts of the system. More energy is in the correct place to produce ejection. Mass mismatch would also account for the decreased intensity of the Ni peak along the <100> direction.

Finally, consider the Al distributions shown in Fig. 5. These distributions are broader than the analogous ones from a pure system. In particular the peak in the <100> direction is not as intense and there is considerable intensity along $\theta = 0°$ which is not observed for first layer ejection from pure Ni. Again, mass mismatch probably accounts for this broadening of the distribution. In general, even considering the approximations in choosing the interaction potentials and in the simple substitution of the Al mass for the Au mass, there is a level of agreement between the experiments shown in Figs 2 and 3 and the simulations shown in Figs 4 and 5.

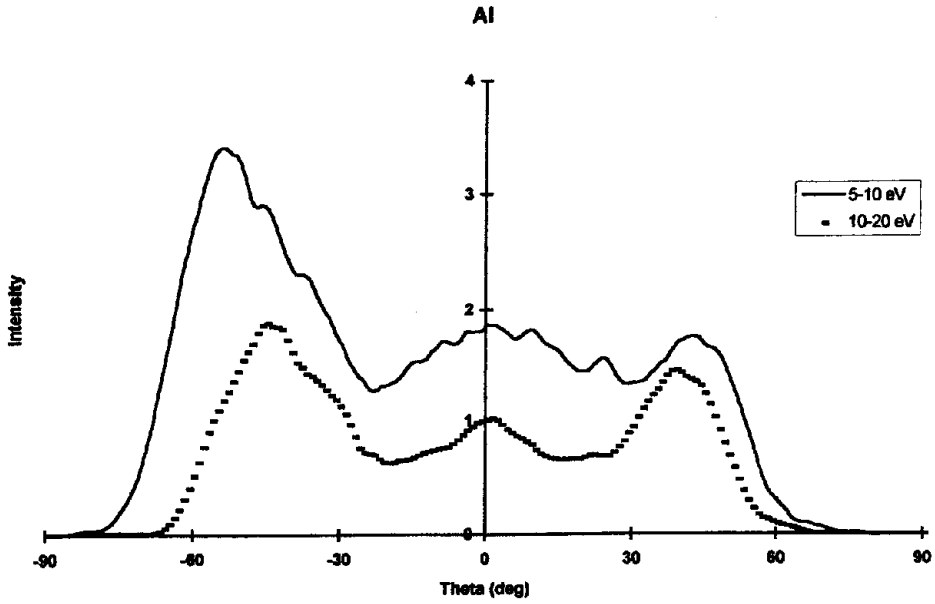

Figure 5. Calculated energy and angle distributions for Al atoms sputtered from Cu_3Au with the Al mass substituted for the Au mass. Directions are the same as in Fig. 2.

CONCLUSIONS

Energy and angle resolved measurements of the Al and Ni atoms sputtered from $Ni_3Al(100)$ show enhanced normal emission when compared to pure Ni(100). The general features of these distributions are well-reproduced by MD calculations of Cu_3Au where the Al mass is substituted for the Au mass. The fact that there is agreement between experiment and theory for these two distinct cases suggest that crystal structure and mass are dominant factors in controlling the sputtering of alloy systems. The MD simulations further show that the enhanced normal emission arises primarily from second-layer Ni atoms ejecting through a ring of first-layer atoms. The results of this initial study suggest that experimental measurement of desorbed-atom trajectories combined with MD simulation will be a valuable approach for elucidating other fundamental aspects of the ion/solid collision event in alloy systems. In addition to addressing the depth of origin problem, for example, more detailed calculations using optimized potential functions should reveal the role of mass mismatches in changing the desorption yield and in broadening polar angle distributions.

Acknowledgements

The authors wish to acknowledge support of the National Science Foundation and the SUR program of the IBM Corporation. Computer assistance was provided by the Center for Academic Computing at Penn State.

REFERENCES

1. Ch. Lehmann and P. Sigmund, *Phys. Stat. Solidi* **16,** 507 (1966).
2. W. O. Hofer, in *Sputtering by Particle Bombardment III*, R. Behrisch and K. Wittmaack (Eds), p. 15, Springer-Verlag, Berlin (1991).
3. N. Winograd, *Mat. Fys. Medd. Dan. Vid. Selsk.* **43,** 223 (1994).
4. R. H. Silsbee, *J. Appl. Phys.* **28,** 1246 (1957).
5. D. E. Harrison Jr., P. W. Kelly, B. J. Garrison and N. Winograd, *Surf. Sci.* **76,** 311 (1978).
6. S. W. Rosencrance, J. S. Burnham, D. E. Sanders, C. He, B. J. Garrison, N. Winograd, Z. Postawa and A. E. DePristo, *Phys. Rev. B* **52,** 6006 (1995).
7. S. W. Rosencrance, N. Winograd, B. J. Garrison and Z. Postawa, *Phys. Rev. B* **53,** 2378 (1996).
8. H. Oechsner, *Int. J. Mass Spectrom. Ion Processes*, **142,** 271 (1995).
9. J. W. Burnett, J. P. Biersack, D. M. Gruen, B. Jorgensen, A. R. Krauss, M. J. Pellin, E. L. Schweitzer and J. T. Yates Jr., *J. Vac. Sci. Tech.* **A6,** 2064 (1988).
10. D. Sondericker, F. Jona and P. M. Marcus, *Phys. Rev. B* **33,** 900 (1986).
11. U. Bardi, P. N. Ross and G. Rovida, *Surf. Sci. Lett.* **205,** L798 (1988).
12. D. G. Re, *The Structure of Surfaces III*, S. Y. Tong, M. A. Van Hove, K. Takayanagi and X. D. Xie, (Eds), Springer Verlag, New York (1991).
13. C. He, Z. Postawa, S. W. Rosencrance, R. Chatterjee, B. J. Garrison and N. Winograd, *Phys. Rev. Lett.* **75(21),** 3950 (1995).
14. P. H. Kobrin, G. A. Schick, J. P. Baxter and N. Winograd, *Rev. Sci. Instrum.* **57,** 1354 (1986).
15. Y. G. Shen, Ph.D. Thesis, University of Newcastle, 1993.
16. Y. G. Shen, D. J. O'Connor and R. J. MacDonald, *Surf. Interface Anal.* **18,** 728 (1992).
17. D. E. Sanders, M. S. Stave, L. S. Perkins and A. E. DePristo, *Comput. Phys. Commun.* **70,** 579 (1992).
18. C. L. Kelchner, D. M. Halstead, L. S. Perkins, N. M. Wallace and A. E. DePristo, *Surf. Sci.* **310,** 425 (1994).
19. S. M. Foiles, M. I. Basekes and M. S. Daw, *Phys. Rev. B* **33,** 7983 (1986).
20. S. P. Chen, A. F. Voter and D. J. Srolovitz, *Scr. Metall.* **20,** 1389 (1986).
21. R. Smith, B. V. King and K. Beardmore, *Rad. Eff. Def. Solids* **141,** 425 (1997).
22. A. Wucher and B. J. Garrison, *Surf. Sci.* **260,** 257 (1992).